Journal of
MATERIALS RESEARCH

Residual stress in ceramics with large thermal expansion anisotropy

S. W. Paulik, M. H. Zimmerman, and K. T. Faber
Department of Materials Science and Engineering, Robert R. McCormick School of Engineering and Applied Science, Northwestern University, Evanston, Illinois 60208-3108

E. R. Fuller, Jr.
National Institute of Standards and Technology, Gaithersburg, Maryland 20899

(Received 10 March 1995; accepted 27 June 1996)

Residual stress was measured in sintered and heat-treated Fe_2TiO_5 samples with various grain sizes. The influence of texturing was assessed by comparing the residual stress states of samples having randomly oriented grains and highly oriented grains produced through magnetically assisted processing. The residual stress was measured with x-ray diffraction using Cr K_α radiation. Due to the significant texture and the consequential oscillations in the $d_{\phi\psi}$ vs $\sin^2\psi$ data, the residual stress was calculated using the Marion–Cohen method. Textured samples showed significantly lower residual stresses except when spontaneous microcracking accompanied grain growth in the randomly oriented systems. Elastic modulus measurements showed a direct correlation between the decrease in residual stress and the microcrack density.

I. INTRODUCTION

Much interest has been focused on the mechanical behavior of single-phase polycrystalline ceramics with large thermal expansion anisotropy.[1–22] Several theories[2–12,22] have been developed to predict the dependence of these properties on grain size. In particular, conditions whereby spontaneous cracking occurs have been defined. Several equations have been derived[2–11,22] describing the critical grain size for spontaneous microcracking in terms of material parameters, having the following general form:

$$l_c^s = \frac{k\gamma_{gb}}{E(\Delta\alpha_{\max}\Delta T)^2}\,, \tag{1}$$

where l_c^s is the grain facet length at the onset of spontaneous microcracking, k is a model dependent constant, γ_{gb} is an isotropic grain boundary surface energy, E is Young's modulus, $\Delta\alpha_{\max}$ is the difference between maximum and average thermal expansion coefficients ($\alpha_{\max} - \overline{\alpha}$), and ΔT is the difference between the strain-free temperature and the temperature of interest. A common element in these studies is the use of a uniform distribution of grain orientations to simulate the thermal expansion mismatch strains inherent in these systems. The critical grain size for spontaneous microcracking can be calculated using Eq. (1); this value, however, applies only to a polycrystalline material with a random distribution of grains.

The residual stress generated during cooling has been estimated by considering two grains with a common boundary in an isotropic matrix. Maximum thermal strain is created when the average coefficient of thermal expansion normal to the shared boundary, $\overline{\alpha}_{12}^{\perp} = (\alpha_1^{\perp} + \alpha_2^{\perp})/2$, is most different from the bulk; i.e., $\overline{\alpha}_{12}^{\perp} = \alpha_{\max}$. The resulting stress in this grain pair is related to the mismatch strains by Hooke's law as follows:

$$\sigma_{\max} = E(\alpha_{\max} - \overline{\alpha})\Delta T\,, \tag{2}$$

where $\sigma_{\max}$ is the stress generated by the maximum thermal expansion mismatch strain. Equations (1) and (2) show that the critical grain size and the maximum stress are governed by the maximum thermal expansion mismatch. This suggests that both may be altered by varying the effective thermal expansion mismatch, which can be done through texturing.

The aim of this study is to examine the effects of grain size and texture on the average residual stresses in Fe_2TiO_5, a highly thermally anisotropic material. X-ray residual stress of a series of control and textured samples were measured and compared. Complementary elastic moduli measurements also were performed to assess microcrack densities in control and textured samples.

II. EXPERIMENTAL PROCEDURE

Samples of Fe_2TiO_5, an orthorhombic pseudobrookite that belongs to the *Bbmm* space group, were fabricated with and without texture by vacuum filtering an Fe_2TiO_5-ethanol suspension in the presence and in the absence of an 8.5-T magnetic field, respectively. The texture is induced by exploiting the anisotropy in the room temperature magnetic susceptibility. (See Table I.) As shown by Farrell *et al.*,[25] the axis with

TABLE I. Selected properties of Fe_2TiO_5.

	Lattice constants[a] (nm)	α[b] (x 10^{-6} K^{-1})	Magnetic susceptibility, χ[c] (× 10^{-3} emu)
a	0.97965	10.1 ± 0.6	3.36
b	0.99805	16.3 ± 0.8	4.11
c	0.37301	0.6 ± 0.1	3.01

[a]Measured at 300 K, from JCPDS-ICDD card 41-1432.
[b]Measured from 300 to 1300 K from Ref. 23.
[c]Extrapolated from data in Ref. 24.

the highest susceptibility, the *b*-axis of Fe_2TiO_5, will align parallel to an applied magnetic field. Samples were then sintered to approximately 94% theoretical density at 1380 °C in air. Selected sintered samples from each system were annealed at 1150 °C for 4, 16, and 64 h for controlled grain growth. This procedure is described in detail elsewhere.[21] These samples will be referred to using the following notation: C and M, for control and magnetically aligned samples, respectively. AS refers to as-sintered and a number, to the number of hours of annealing time; e.g., MAS represents the as-sintered magnetically aligned material. Surfaces with normals parallel to the anticipated alignment direction were finished by grinding with 600 grit SiC to obtain a flat surface, and then polishing with 0.3 μm Al_2O_3 to minimize pullout.

X-ray diffraction was performed on a Picker diffractometer using Cr K_α radiation at 40 kV and 30 mA in-line focus.[26] A graphite monochromator was placed in the diffracted beam to remove fluorescence of the titanium caused by the Cr radiation. The source slit had a 1° divergence while the receiving slit had a 0.076° divergence. The beam size was approximately 2.5 by 14.5 mm.

The average residual stress state was determined by measuring the interplanar spacing of the (262) peak, located at 144.2° 2θ, as shown in Fig. 1. This peak was chosen because the high angle provides sufficiently small calculation errors and no overlapping peaks are present. The diffraction geometry is depicted in Fig. 2, where ψ describes the angle between the surface normal and the diffraction vector. The value of ψ was varied from 0° to 45° using Ω-goniometry. The peak profile was measured from 143.010° to 145.985° 2θ in 0.025° steps and for counting times of 720 s. The K_{α_1} and K_{α_2} peaks were deconvoluted by describing the doublet as a pseudo-Voigt function, whose secondary peak is half as intense as the primary peak.

Impurities of hematite, Fe_2O_3, were present in concentrations of 8 vol. % in all of the Fe_2TiO_5 samples (see Ref. 21). Their influence on residual stress was ignored because the grain size of the Fe_2O_3 is small with respect to the Fe_2TiO_5 grains. Thermal mismatch stresses fall off as $1/r^3$, where r is the distance from the Fe_2O_3 grain, and are negligible over the bulk of the Fe_2TiO_5 grains.

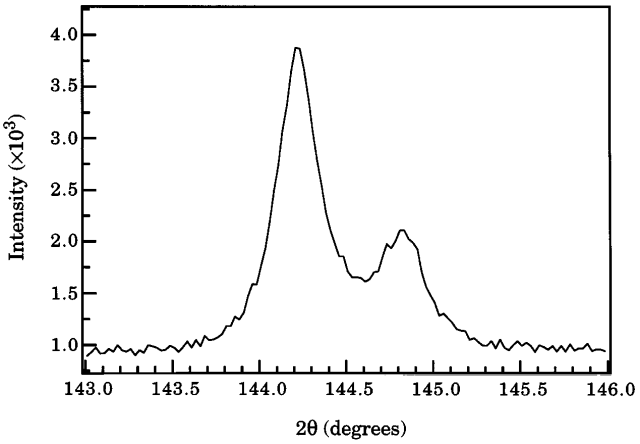

FIG. 1. Peak profile of the (262) used for the residual stress measurements.

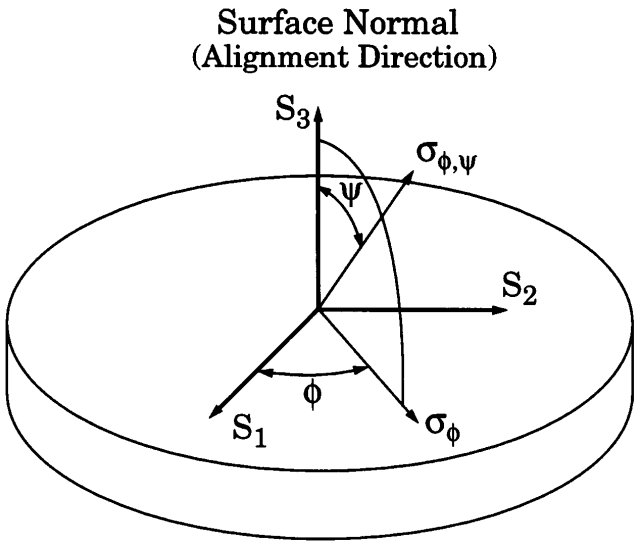

FIG. 2. Schematic diagram of the sample surface illustrating the angles ϕ and ψ with respect to the surface normal.

Measurement of d_0, the unstressed lattice constant, was performed using the standard $\sin^2\psi$ method[26,27] on a powder sample annealed for 20 min at 900 °C. Samples were mounted on a rotating stage with the sample surface parallel to and intersecting the axis of rotation, such that the normal of the sample surface is parallel to the diffraction vector. The standard $\sin^2\psi$ technique involves measuring the d-spacing as the sample surface is rotated about the ψ axis. This was done at angles of 0.00, 18.43, 26.57, 33.21, 39.23, and 45.00°. These results were also used to confirm the alignment of the diffractometer.

Elastic moduli were measured using a pulse-echo technique. Using a 50 MHz longitudinal wave transducer and a 25 MHz shear wave transducer, the time required for a given pulse to traverse twice the sample thickness

was measured. These values, in combination with the sample density as measured by Archimedes' method, allowed the calculation of the bulk, shear, and Young's moduli and Poisson's ratio, as shown in the following:

$$B = \rho\left(\vartheta_1 - \frac{4}{3}\vartheta_s\right) \tag{3}$$

$$G = \rho\vartheta_s^2 \tag{4}$$

$$E = 2(1 + \nu)G \tag{5}$$

$$\nu = \frac{2 - \left(\frac{\vartheta_l}{\vartheta_s}\right)^2}{2\left(1 - \left(\frac{\vartheta_l}{\vartheta_s}\right)^2\right)} \tag{6}$$

where B is the bulk modulus, ρ is the sample density, ϑ_l is the longitudinal wave velocity, ϑ_s is the shear wave velocity, G is the shear modulus, and ν is Poisson's ratio.[28]

III. RESIDUAL STRESS ANALYSIS

In the absence of surface normal stresses, biaxial stress measurements may be used to characterize the residual stresses present in a material.[27,29] The classical x-ray residual stress equation describing this follows:

$$\frac{d_{\phi\psi} - d_0}{d_0} = \frac{1 + \upsilon}{E}\sigma_\phi \sin^2\psi - \frac{\upsilon}{E}(\sigma_{11} + \sigma_{22}), \tag{7}$$

where $d_{\phi\psi}$ is the d-spacing at a given ϕ and ψ angle, d_0 is the unstressed lattice spacing, υ and E are the appropriate elastic constants, σ_{ii} is the stress component along the S_i direction, and σ_ϕ is the stress component along the S_ϕ direction ($= \sigma_{11}\cos^2\phi + \sigma_{22}\sin^2\phi$).[27] These are shown schematically in Fig. 2 for the orthonormal surface coordinate system S_i. Equation (7) predicts a linear relationship in $d_{\phi\psi}$ vs $\sin^2\psi$.[26,27] If the stresses are uniformly distributed within the plane of the surface, i.e., σ_{11} equals σ_{22}, then σ_ϕ will be independent of ϕ and will characterize the residual stress in the material.

When a sample exhibits preferred orientation and large elastic anisotropy, nonuniformly distributed microstresses are produced by the texture.[27,29–32] As a result, the relation between $d_{\phi\psi}$ and $\sin^2\psi$ is not linear; rather, $d_{\phi\psi}$ vs $\sin^2\psi$ will oscillate about a line that describes the macrostress. These oscillations are essentially the superposition of the textured-induced microstresses and the linear macrostresses, as shown in Fig. 3 for sample M16. The Marion–Cohen method[27,29] provides a means of analyzing $d_{\phi\psi}$ and $\sin^2\psi$ data with oscillations produced by sample texture. This method allows the deconvolution of the linear residual stress from the nonlinear textural stresses, as schematically illustrated in Fig. 4.

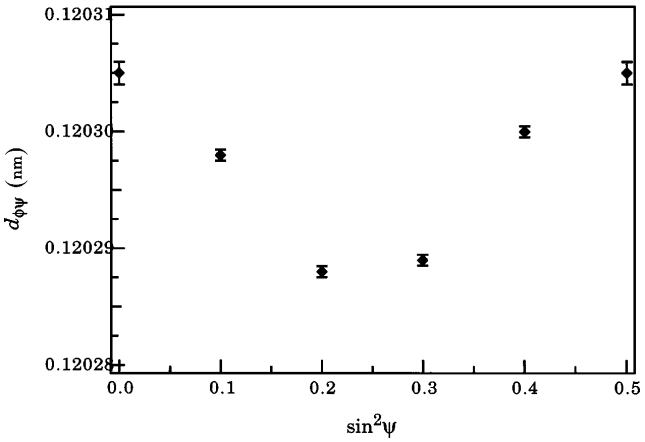

FIG. 3. Typical $d_{\phi\psi}$ vs $\sin^2\psi$ data illustrating the oscillations induced by the nonuniform response to stress in a textured sample (M16).

The Marion–Cohen analysis assumes that the inhomogeneous distribution in residual strains is caused by the given plane having a nonuniform response to stress. This strain distribution results in a dependence of the interplanar spacings on the texture. Specifically, the variations in the d-spacing of a given plane, d_T, can be related to the local texture with respect to the surface normal. The texture and, therefore, d_T can be characterized by the change in intensity of the specific *hkl* plane with respect to the surface coordinate system as in the following:

$$d_T = (d_A - d_B)\cdot f(\alpha,\beta) + d_B, \tag{8}$$

where d_A and d_B define the range over which the d-spacing varies and $f(\alpha,\beta)$ is the distribution function of the given plane relative to the sample coordinates and the angles α and β, as illustrated in Fig. 5. The presence of these textural stresses obscures the true location of d_0 at $\psi = 0.00$. If the stresses are assumed to be uniformly distributed in the plane, the following relation describing the variation in $d_{\phi\psi}$ with $\sin^2\psi$ in the presence of texture[27,29] results:

$$d_{\phi\psi} = (d_{\phi\psi_A} - d_{\phi\psi_B})\cdot f(\alpha,\beta) + d_0 \cdot \frac{(1 + \upsilon)}{E}\sigma_\phi \sin^2\psi + d_{\phi\psi_B}, \tag{9}$$

where it is assumed that the stresses contributing to σ_ϕ yield a linear $d_{\phi\psi}$ vs $\sin^2\psi$ dependence. Therefore, measuring $f(\alpha,\beta)$, which can be taken as the normalized integrated or maximum peak intensity, and $d_{\phi\psi}$ as a function of ψ for a particular ϕ, allows the calculation of $d_{\phi\psi_A}$, $d_{\phi\psi_B}$, and σ_ϕ.[27,29] For these experiments α equaled 0° and β equaled ψ, or $f(\alpha,\beta) = f(0,\psi)$.

For each specimen, $f(0,\psi)$ was determined by fitting the normalized integrated intensity vs $\sin^2\psi$ with a fourth order polynomial, a Gaussian, and a Lorentzian function. The best fit, as defined by the χ^2 value closest

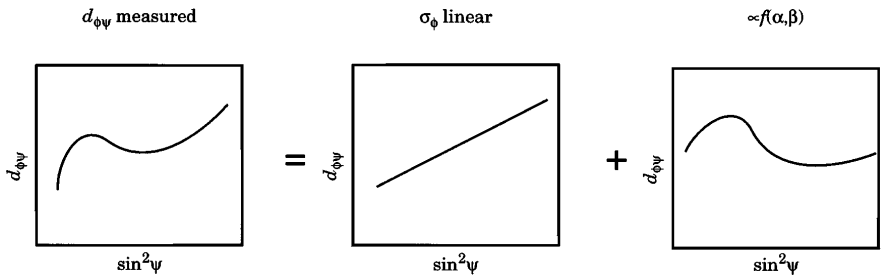

FIG. 4. Schematic diagram illustrating the superposition principle employed by the Marion–Cohen method.

to the number of data points in the fit,[33] was then used in Eq. (9) to fit $d_{\phi\psi}$ vs $\sin^2\psi$, determining the value of σ_ϕ. It should be noted that values of σ_ϕ were calculated using the isotropic elastic constants and are therefore labeled σ_ϕ^{iso}. This assumption is legitimate for the control samples which have little or no crystallographic texture. The assumption is less appealing for the magnetically aligned material, but will provide the trends in residual stress with annealing time for comparison. The full compliance matrix or x-ray elastic constants needed for accurate σ_ϕ calculation for the textured materials are not available.

IV. RESULTS AND DISCUSSION

Measurement of the unstressed d-spacing of an annealed powder established the invariance of $d_{\phi\psi}$ with $\sin^2\psi$ in the absence of residual stress, as shown in Fig. 6. From this one can infer that oscillations found in the $d_{\phi\psi}$ vs $\sin^2\psi$ for the sintered specimens, as shown in Fig. 3, are texturally induced microstresses. The value of d_0 obtained from this is 0.120300 ± 0.000001 nm. This value of uncertainty represents the standard deviation from statistics associated with each point used in the pseudo-Voigt fit. In order to apply the Marion–Cohen analysis one needs to fit the data with this uncertainty. Additional uncertainties are inherent with each measurement, including horizontal and vertical divergence, specimen displacement, and y-axis displacement which are estimated at a maximum $-0.0063°$ or $\pm 0.0051°$ 2θ which lead to -12.5 and 10.2 MPa in σ_ϕ.[26,28,34]

A typical $f(0,\psi)$ vs $\sin^2\psi$ function for the control series is shown in Fig. 7(a), while the subsequent fit for $d_{\phi\psi}$ vs $\sin^2\psi$ is shown in Fig. 7(b), yielding a residual stress of 45.1 ± 5.8 MPa. The $f(0,\psi)$ distribution for control series tended to decrease with increasing $\sin^2\psi$, where a constant $f(0,\psi)$ with $\sin^2\psi$ would be expected for a sample with a uniform distribution of grain orientations. The magnetically aligned samples maintained a similarly shaped $f(0,\psi)$ vs $\sin^2\psi$ distribution throughout the series. A typical $f(0,\psi)$ vs $\sin^2\psi$ distribution for the magnetically aligned series is shown in Fig. 8(a), and the resulting fit to $d_{\phi\psi}$ vs $\sin^2\psi$ is shown in Fig. 8(b), yielding a residual stress of 26.9 ± 2.1 MPa. For ideal b-axis alignment the $f(0,\psi)$ vs $\sin^2\psi$ distribution would be single-valued at 19.3° ψ, as illustrated by the dotted line in Fig. 8(a) and shown schematically in Fig. 9(a). A distribution like that observed in Fig. 8(a) would be expected for a microstructure that possesses a distribution of b-axes about the alignment axis, as illustrated in Fig. 9(b). The maximum in the $f(0,\psi)$ vs $\sin^2\psi$ distribution in Fig. 8(a), between 26° and 33° ψ, suggests a possible misorientation of the b-axis between 5° and 10° off the surface normal. The maximum for the magnetically

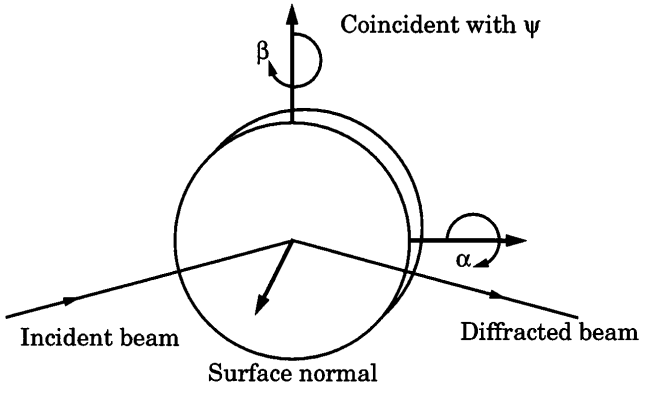

FIG. 5. Schematic diagram depicting sample surface relative to the diffracting plane and the angles α and β (after Ref. 25).

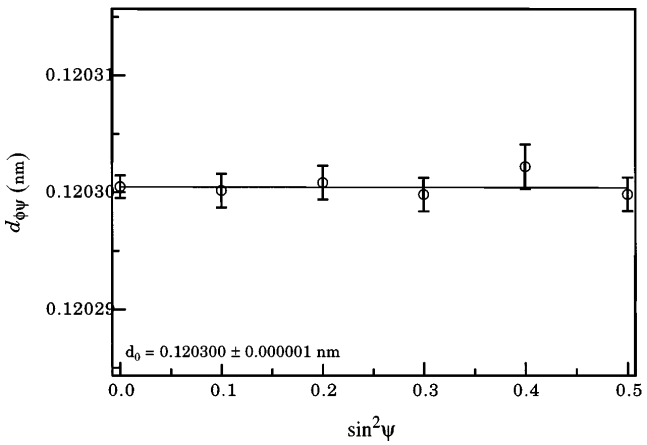

FIG. 6. The unstressed lattice spacing, d_0, as a function of $\sin^2\psi$, showing the alignment of the diffractometer and a linear $d_{\phi\psi}$ vs $\sin^2\psi$ relation in the absence of residual stress.

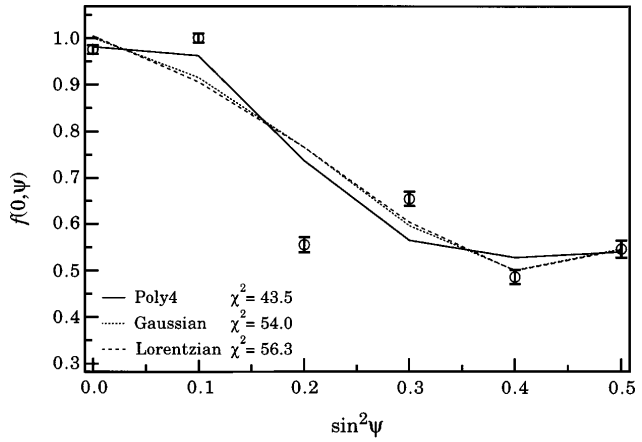

(a)

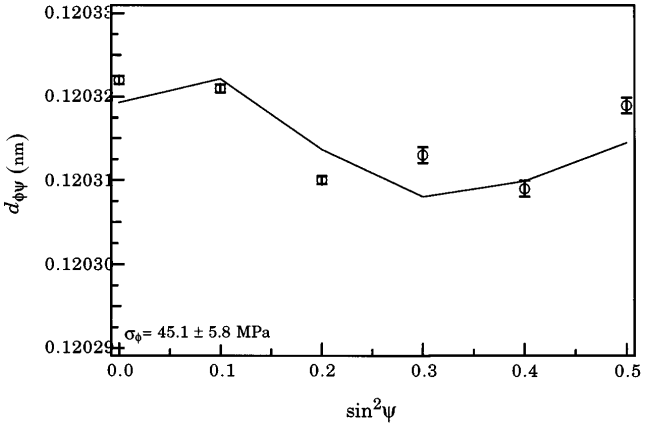

(b)

FIG. 7. An example of (a) the $f(0,\psi)$ distribution vs $\sin^2\psi$ and (b) the calculated $d_{\phi\psi}$ vs $\sin^2\psi$ using the Marion–Cohen method for a control sample (C4).

aligned series varied between approximately 20° and 30° ψ.

The residual stress values for the control and magnetically aligned series are shown in Fig. 10. Comparing as-sintered samples from the control and magnetically aligned series shows that b-axis alignment has created a 70% reduction in residual stress. This establishes that the texture induced by the magnetic field-assisted processing has resulted in a substantial reduction in residual strain.

With increasing grain size, the residual stress in the control samples decreases precipitously, by more than 67% from the as-sintered state to the 4 h annealed material, where the average grain size is approximately 9 μm. Near complete residual stress relief is accomplished at the largest grain size examined. A possible interpretation is that an increasing number of spontaneous microcracks are generated with grain size. As the number and/or size of microcracked grain boundaries increases, the amount of stored elastic strain released increases, resulting in a decrease in the average residual stress.

Examining the magnetically aligned series, the trend is also to a decreasing residual stress with increasing grain size, but the relative magnitude of the decrement is substantially smaller. This reduced decrement might be interpreted as a reduction in the number of spontaneous microcracks that are generated with increasing grain size when compared to the control series.

An estimate of the expected average residual stress for a given plane in an unmicrocracked material with a uniform distribution of grains can be made by re-examining Eq. (2) for a single grain with respect to the particular plane as follows:

$$\sigma_{hkl} = E_{hkl}(\alpha_{hkl} - \overline{\alpha})\Delta T\,, \qquad (10)$$

where the subscript indicates the property normal to the *hkl* plane, σ_{hkl} is the average thermal mismatch stress, and $\overline{\alpha}$ is the average thermal expansion for

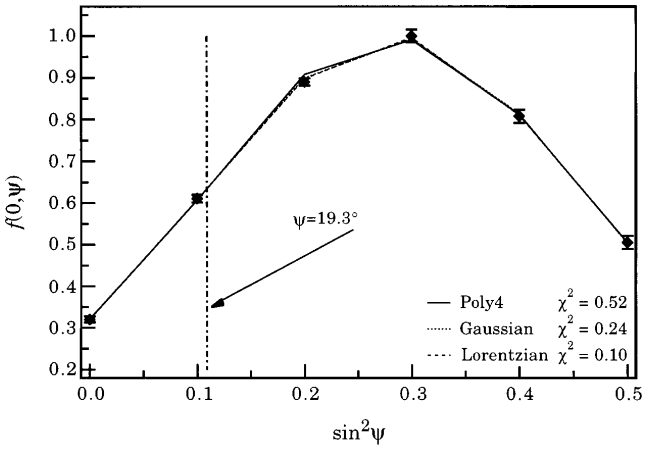

(a)

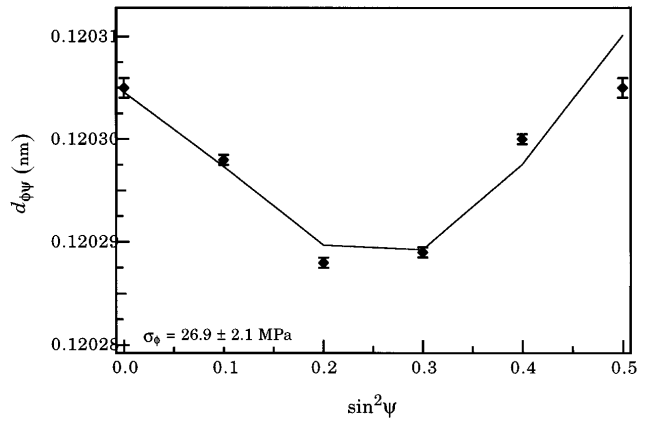

(b)

FIG. 8. A typical (a) $f(0,\psi)$ distribution vs $\sin^2\psi$ and (b) the calculated $d_{\phi\psi}$ $\sin^2\psi$ curve using the Marion–Cohen method for the magnetically aligned series (M16).

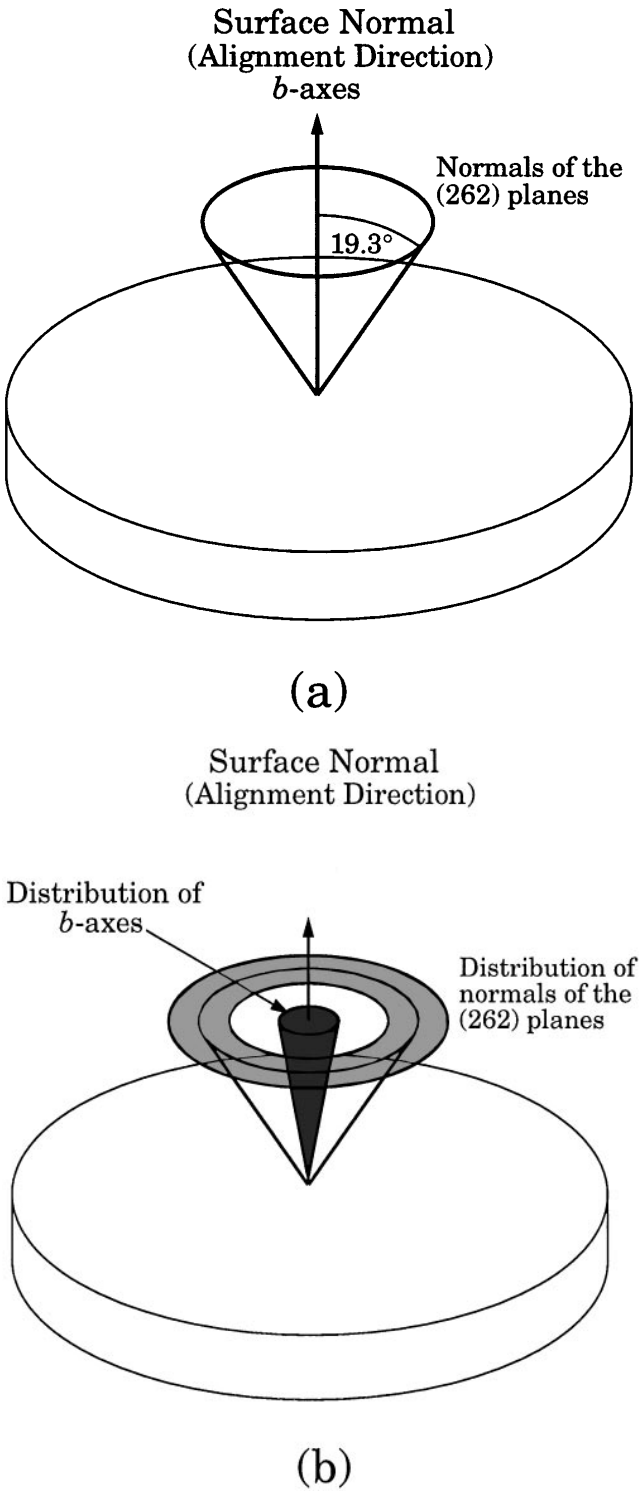

FIG. 9. Distribution of (262) plane normals for a sample with (a) ideal b-axis alignment and (b) a distribution of b-axes about the alignment direction.

a uniform distribution of grains. Because the elastic constants for Fe_2TiO_5 are not available, the isotropic Young's modulus, 180 GPa,[4,8] will be substituted for E_{hkl}.

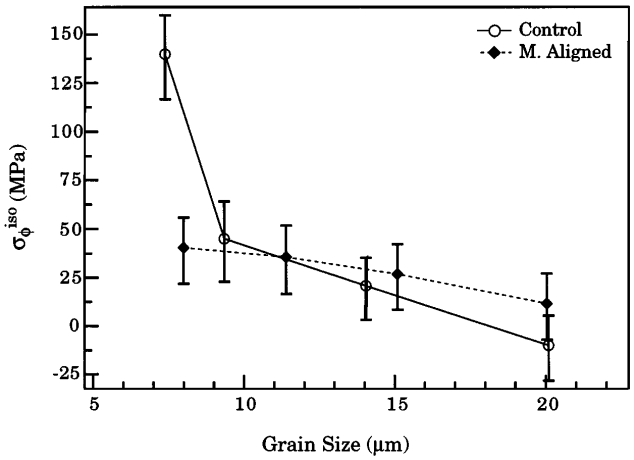

FIG. 10. The average residual stress, σ_ϕ^{iso}, normal to the (262) plane calculated from isotropic elastic constants as a function of the average grain size on disk surfaces.

For the thermal expansion mismatch strain, ΔT may be estimated at 1000 °C. From the values in Table I, α is $9.00 \cdot 10^{-6}$/°C. α_{262} can be estimated from the tensor properties of thermal expansion by using the following equation:

$$\alpha_{hkl} = \alpha_{h00} l_1^2 + \alpha_{0k0} l_2^2 + \alpha_{00l} l_3^2 , \qquad (11)$$

where l_i are the direction cosines of the hkl plane.[35] Substituting the direction cosines of the (262) plane for orthorhombic Fe_2TiO_5 into Eq. (11) yields a value of $15.49 \cdot 10^{-6}$/°C for α_{262}. Using this value in Eq. (9), along with the other pertinent parameters, i.e., $E_{hkl} =$ 180 GPa, results in a value of 1.17 GPa for σ_{262}^R, the average residual stress normal to the (262) plane for an unmicrocracked, polycrystalline sample with a uniform distribution of grain orientations. Comparing this to the value obtained for the as-sintered sample of 139.9 MPa implies that these samples have already spontaneously microcracked. With a grain size of approximately 7.5 μm in the as-sintered samples, where the reported critical grain size for spontaneous microcracking in Fe_2TiO_5 is 3 to 5 μm,[4,6] the presence of spontaneous microcracks is expected. Additionally, the trend in the residual stress curve suggests that extrapolating to smaller grain sizes would result in a significant increase in residual stress.

In order to estimate the average residual stress for an unmicrocracked, b-axis aligned specimen, the average coefficient of thermal expansion, α_T, seen by the (262) planes in the textured microstructure must be determined. A first order approximation can be made by considering planes whose normals lie within a cone of half angle of 20° from the 262 axis, taken at 20° from the b-axis [a maximum in the $f(0, \psi)$ distribution]. α_T can then be estimated by considering all the planes

from a theoretical x-ray powder pattern, and averaging the coefficients of thermal expansion of all those planes within the prescribed cone, which yields a value of α_T of $14.95 \cdot 10^{-6}/°C$. Substituting this value into Eq. (10) obtains 97.2 MPa for σ^T_{262}, the average residual stress normal to the (262) for an unmicrocracked polycrystalline sample with *b*-axis alignment. This predicted value suggests that *b*-axis texturing provides a significant reduction in residual stress normal to the (262). This value is of the order of the experimental value obtained for the magnetically aligned sample of 40.4 MPa. From the trends of residual stress vs grain size, a slightly higher residual stress may be obtained with a reduction in initial grain size.

These results provide an indirect measure of the microcracking in the material, since the x-ray residual stress is a measure of the average residual stress and does not indicate the maximum value. Elastic modulus measurements, however, when coupled with the appropriate analyses or assumptions, provide a direct measure of the number of microcracks in a specimen. The measured Young's and shear moduli for these materials are shown in Figs. 11(a) and 11(b), respectively. Figure 11(d) shows the dependence of the bulk modulus on the average grain size. The control samples exhibit a significant reduction in moduli with increasing grain size.

From these changes in elastic moduli, a microcrack density parameter can be calculated by applying the analysis of Budiansky and O'Connell.[36] They related the elastic moduli to the degree of microcracking in a sample through a microcrack density parameter, ϵ, for randomly oriented circular cracks, as shown in the following equation for the bulk modulus:

$$\frac{B_m}{B} = 1 - \frac{16}{9}\left(\frac{1 - \upsilon_m^2}{1 - 2\upsilon_m}\right)\epsilon\,, \qquad (12)$$

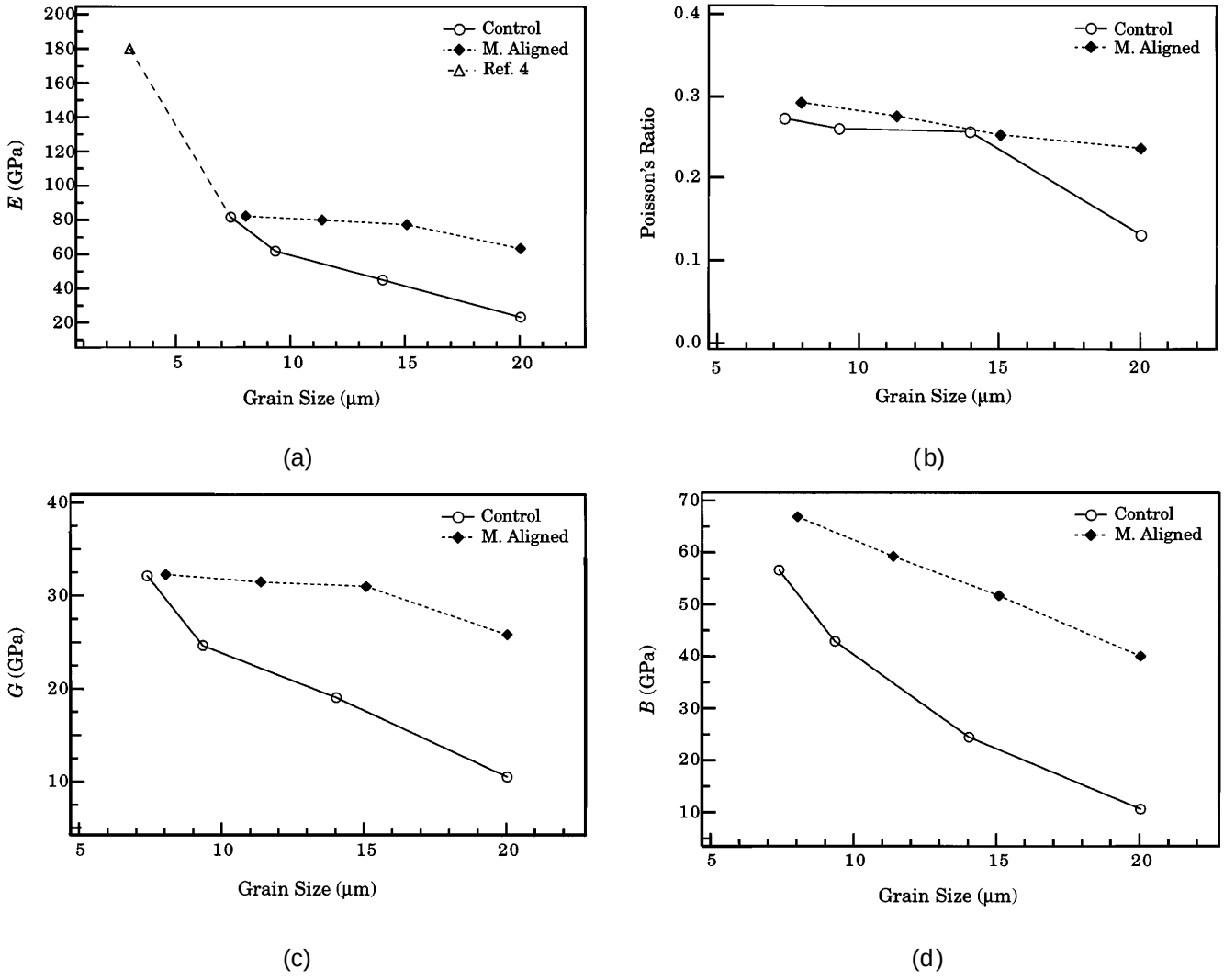

FIG. 11. (a) Young's modulus, *E*, (b) Poisson's ratio, (c) the shear modulus, *G*, and (d) the bulk modulus, *B*, parallel to the surface normal and direction of the magnetic field as a function of grain size.

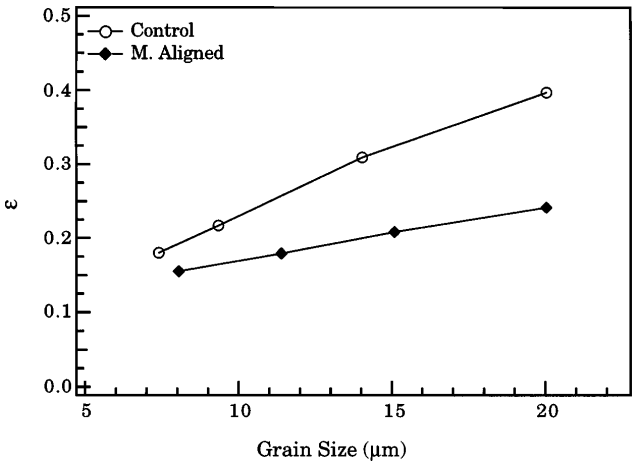

FIG. 12. The microcrack density parameter, ϵ, as a function of grain size.

where the subscript m indicates the microcracked body, B is the bulk modulus, and $\epsilon = N_V\langle c^3\rangle$ where N_V is the number of microcracks/unit volume and c is the microcrack radius. The bulk modulus incorporates both the shear and longitudinal properties, as shown in Eq. (3). Additionally, the theoretical bulk modulus, B_T, is readily calculated and can be used to represent the unmicrocracked state. Ledbetter, using an ionic model[37] based on the space group ($Bbmm$) and atom positions, calculated $B_T = 169.9$ GPa for Fe_2TiO_5.[38]

The value of ϵ for both series was calculated using Eq. (12) by replacing B and B_T. While B is expected to vary with texture, B_T is used for both the control and magnetically aligned series to obtain an estimate of ϵ. The dependence of ϵ on the average grain size of the surface of the disks is shown in Fig. 12. Since in spontaneously microcracking systems the crack size is of the order of the grain facet size,[39] these results indicate that the percentage of microcracked grains in the control samples far exceeds that in the textured materials, particularly at long annealing times. The magnetically aligned samples also exhibit a reduction in moduli with increasing grain size, but at a substantially reduced rate, again, consistent with the residual stress results. The moduli of all the magnetically aligned samples are larger than those for even the shortest annealing time of the control samples. These results are a direct link between the induced b-axis alignment and reduced residual stress, causing a significant reduction in spontaneous microcracking and increased grain size tolerance.

As Fig. 11 illustrates, the elastic moduli of the CAS and MAS samples are equivalent. Extrapolating the trends, however, suggests that the moduli of the control series would increase significantly with a small reduction in grain size, while the magnetically aligned system appears to be close to the maximum value. The isotropic Young's modulus of 180 GPa could be the end point of the control curve at smaller grain sizes. The trends in elastic moduli mirror the behavior seen in the residual stress measurements and confirm that microcracking is responsible for the reduction in residual stress with increasing grain size.

V. SUMMARY

Fe_2TiO_5 samples exhibited nonlinear $d_{\phi\psi}$ vs $\sin^2\psi$ behavior during x-ray residual stress measurements which were analyzed by the Marion–Cohen method. The residual stress normal to the (262) plane in the control samples was significantly larger than that in the magnetically aligned samples except when substantial microcracking accompanied grain growth. The residual stress decreased with increasing grain size as the number of microcracks increased. Comparison of samples in the as-sintered state showed that the residual stress in magnetically aligned material was less than 30% of that in the control material. Theoretical calculations for unmicrocracked bodies predicted a decrease in residual stress of over 90% by b-axis alignment.

As a complementary measure, the elastic moduli of these samples were determined to provide a measure of the relative degree of microcracking. By coupling the elastic measurements with the analysis of Budiansky and O'Connell,[36] the microcrack density parameter was calculated. With increasing grain size the density of microcracks increased in both the control and magnetically aligned materials, but at a considerably reduced rate in the magnetically aligned material. The b-axis alignment induced by magnetic field processing effectively controls the thermal expansion mismatch, reducing the propensity toward microcracking and providing increased grain size tolerance.

ACKNOWLEDGMENTS

Funding for this work was provided by the National Science Foundation under Grant Nos. DMR-9100035 and DMR-9411477. Jonathan Almer provided valuable assistance in the residual stress measurements.

REFERENCES

1. W. R. Buessem and F. F. Lange, Interceram. **15** (3), 229–231 (1966).
2. R. W. Davidge and G. Tappin, J. Mater. Sci. **3**, 297–301 (1968).
3. J. A. Kuszyk and R. C. Bradt, J. Am. Ceram. Soc. **56** (8), 420–423 (1973).
4. J. J. Cleveland and R. C. Bradt, J. Am. Ceram. Soc. **61** (11–12), 478–481 (1978).
5. A. G. Evans, Acta Metall. **26**, 1845–1853 (1978).
6. E. D. Case, J. R. Smyth, and O. Hunter, J. Mater. Sci. **15**, 149–153 (1980).
7. D. R. Clarke, Acta Metall. **28**, 913–924 (1980).
8. R. W. Rice and S. W. Freiman, J. Am. Ceram. Soc. **64** (6), 350–354 (1981).
9. R. W. Davidge, Acta Metall. **29**, 1695–1702 (1981).

10. Y. Fu and A. G. Evans, Acta Metall. **33**, 1515–1523 (1985).
11. Y. Ohya, Z. Nakagawa, and K. Hamano, J. Am. Ceram. Soc. **70** (8), C-184–C-186 (1987).
12. V. Tvergaard and J. W. Hutchinson, J. Am. Ceram. Soc. **66** (3), 157–166 (1988).
13. H. J. Siebeneck, D. P. H. Hasselman, J. J. Cleveland, and R. C. Bradt, J. Am. Ceram. Soc. **59** (5–6), 241–244 (1976).
14. R. W. Rice and R. C. Pohanka, J. Am. Ceram. Soc. **62** (11–12), 559–563 (1979).
15. E. D. Case, J. R. Smyth, and O. Hunter, Jr., Mater. Sci. Eng. **51**, 175–179 (1981).
16. N. Claussen, B. Mussler, and M. V. Swain, J. Am. Ceram. Soc. **65** (1), C-14–C-16 (1982).
17. J. E. Blendell and R. L. Coble, J. Am. Ceram. Soc. **65** (3), 174–178 (1982).
18. Y. Fu and A. G. Evans, Acta Metall. **33** (8), 1525–1531 (1985).
19. J. W. Hutchinson, Acta Metall. **35** (7), 1605–1619 (1987).
20. H. A. J. Thomas and R. Stevens, Br. Ceram. Trans. J. **88**, 144–151 (1989).
21. S. W. Paulik, K. T. Faber, and E. R. Fuller, Jr., J. Am. Ceram. Soc. **77** (2), 454–458 (1994).
22. R. C. Bradt, in *Low-Expansion Materials*, edited by D. P. Stinton and S. Y. Limaya (Ceramic Transactions, Westerville, OH, 1995), Vol. 52, p. 5.
23. G. Bayer, J. Less-Common Met. **24**, 129–138 (1971).
24. U. Atzmony, G. Gorodetsky, E. Gurewitz, E. Hermon, R. M. Hornreich, M. Melamud, H. Pinto, H. Shaked, S. Shtrikman, and B. Wanklyn, J. Magn. Magn. Mater. **15–18**, 115–116 (1980).
25. D. E. Farrell, B. S. Chandrasekhar, M. R. DeGuire, M. M. Fang, V. G. Kogan, J. R. Clem, and D. K. Finnemore, Phys. Rev. B **36** (7), 4025–4027 (1987).
26. D. B. Cullity, *Elements of X-ray Diffraction*, 2nd ed. (Addison-Wesley, Reading, MA, 1978).
27. I. C. Noyan and J. B. Cohen, *Residual Stress, Measurement by Diffraction and Interpretation* (Springer-Verlag, New York, 1987).
28. E. Schreiber, O. L. Anderson, and N. Soga, *Elastic Constants and Their Measurements* (McGraw-Hill, New York, 1973).
29. R. H. Marion and J. B. Cohen, Adv. X-ray Anal. **18**, 466–501 (1975).
30. B. D. Cullity, Adv. X-ray Anal. **20**, 259–271 (1977).
31. C. M. Brakman and P. Penning, Acta Crystallogr. A **44**, 163–167 (1988).
32. C. M. Brakman, Th. H. de Keijser, N. M. van der Pers, P. Penning, and S. Radelaar, Philos. Mag. A **58** (4), 635–650 (1988).
33. W. H. Press, B. P. Flannery, S. A. Teukolsky, and W. T. Vetterling, *Numerical Recipes in C, The Art of Scientific Computing* (Cambridge University Press, New York, 1988).
34. M. R. James and J. B. Cohen, Adv. X-ray Anal. **20**, 291–307 (1977).
35. J. F. Nye, *Physical Properties of Crystals* (Oxford University Press, Oxford, G. B., 1957).
36. B. Budiansky and R. J. O'Connell, Int. J. Solids Struct. **12**, 81–97 (1976).
37. D. Balzar and H. Ledbetter, Am. Miner. **78**, 1192–1196 (1993).
38. H. Ledbetter, private communication, February 1994.
39. E. D. Case and C. J. Glinka, J. Mater. Sci. **19**, 2962–2968 (1984).